

Optimized Contact Plan Design for Reflector and Phased Array Terminals in Cislunar Space Networks

Huan Yan^{*}, Juan A. Fraire^{†‡}, Ziqi Yang^{*}, Kanglian Zhao^{*}, Wenfeng Li^{*}, Yuan Fang^{*},
Jinjun Zheng[§], Chengbin Kang[§], Huichao Zhou[§], Xinuo Chang[§], Lu Wang[§], Linshan Xue[§],

^{*}Nanjing University, Nanjing, China

[†]Inria, INSA Lyon, CITI, UR3720, 69621 Villeurbanne, France

[‡]CONICET – Universidad Nacional de Córdoba, Córdoba, Argentina

[§]China Academy of Space Technology(CAST)

Abstract—Cislunar space is emerging as a critical domain for human exploration, requiring robust infrastructure to support spatial users—spacecraft with navigation and communication demands. Deploying satellites at Earth-Moon libration points offers an effective solution. This paper introduces a novel Contact Plan Design (CPD) scheme that considers two classes of cislunar transponders: Reflector Links (RL) for high-volume data transfer and Phased Array Links (PL) for fast switching and navigation services. Our approach addresses the needs of both satellites and spatial users within the Earth-Moon Libration Point Communication and Navigation Constellation (EMLP-CNC). Simulations validate the proposed scheme, demonstrating its effectiveness in serving spatial users while meeting satellite ranging and communication requirements. These findings provide essential insights for developing future Cislunar Space Infrastructures.

Index Terms—Cislunar Space Infrastructure, libration points, contact plan design (CPD).

I. INTRODUCTION

The increasing momentum of lunar and deep space exploration drives a surge in missions across Cislunar space [1], [2]. In this context, spatial users—spacecraft requiring communication and navigation support—face critical challenges. Due to the limitations imposed by orbital height, Earth-orbit satellite navigation systems, such as GNSS, fail to effectively serve users operating beyond medium and high Earth orbits [3], [4]. This underscores the pressing need for a dedicated Cislunar Space Infrastructure to support operations within this domain reliably [5]–[7].

Libration points are regions in space where the gravitational forces of two massive celestial bodies, such as the Earth and the Moon or the Earth and the Sun, balance with the centripetal force acting on a smaller third object [8]. These equilibrium points, designated L1 through L5, enable the smaller object to maintain a stable relative position. Deploying satellites at the Earth-Moon libration points forms the basis for a robust Cislunar Space Infrastructure [9], [10], which can deliver critical services to users operating in this region [11], [12]. Key advantages include comprehensive coverage of Cislunar space [13], reduced fuel requirements for orbit control, and seamless integration with Earth’s satellite communication and navigation systems [14]. These features underscore the transformative potential of the Earth-Moon Libration Point Communication and Navigation Constellation (EMLP-CNC)

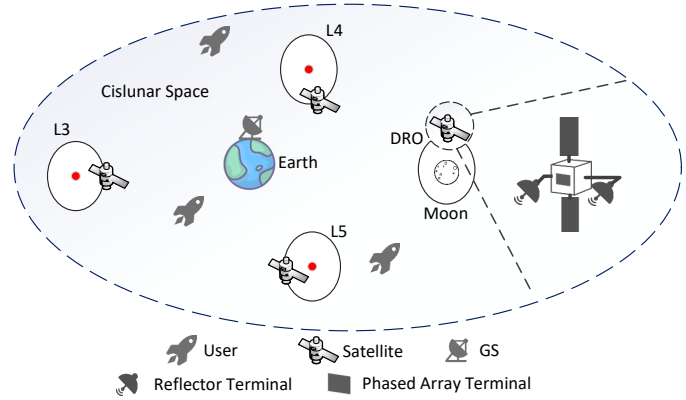


Fig. 1. Cislunar Space Networks: Earth-Moon Libration Point Communication and Navigation Constellation (EMLP-CNC)

for supporting future deep-space missions. As illustrated in Fig.1, EMLP-CNC comprises satellites stationed at the L3, L4, and L5 libration points, as well as in distant retrograde orbits (DRO) around the Moon [9]. These satellites interact with Earth’s spatial users and ground stations (GSs).

The satellites in EMLP-CNC are equipped with two distinct types of transponders: reflector terminals [15] and phased array terminals [16]. Reflector terminals utilize parabolic reflectors to concentrate signals and rely on mechanical rotation for precise but relatively slow alignment, enabling reflector links (RLs) formation. In contrast, phased array terminals consist of numerous small antennas capable of electronically steering beams by controlling signal phase and amplitude, enabling the creation of phased array links (PLs) that adjust direction and strength with greater agility. In EMLP-CNC, reflector terminals, with diameters of several meters [17], [18], deliver significantly higher antenna gain and data rates than phased array terminals. However, they are constrained by their mechanical steering, which limits link-switching speeds and reduces the frequency of topology changes. Conversely, phased array terminals excel in rapid link switching and dynamic topology adjustments due to their electronic beam-steering capabilities. Table I summarizes these critical differences, highlighting the need for distinct CPD schemes to manage RLs and PLs in the EMLP-CNC effectively.

TABLE I
KEY CHARACTERISTICS OF RL AND PL

	Date Rate	Swing Speed
RL	High (≈ 10 Mbps)	Low (≈ 0.3 Deg/s)
PL	Low (≈ 10 Kbps)	High (Immediate)

Orbital mechanics dictate that establishing links, or contacts, between space nodes is predictable and intermittent. Selecting a subset of these contacts to optimize system performance under resource constraints is termed Contact Plan Design (CPD) [19]–[22]. Historically, CPD efforts have concentrated on fulfilling the ranging and communication requirements of satellites [23]–[33], often neglecting the distinct demands of spatial users. These users exhibit temporally driven and mission-specific communication needs, presenting challenges that existing CPD frameworks fail to address adequately. Furthermore, existing CPD schemes have not considered the liberation point topologies in Cislunar networks nor the characteristics of constituent RL and PL in future Cislunar communication systems.

To address this gap, we explore CPD schemes designed to serve spatial users within the EMLP-CNC framework. To the best of our knowledge, this work is the first to propose and solve a CPD scheme that integrates RLs and PLs to simultaneously meet satellites’ ranging and communication needs and the service demands of spatial users in a Cislunar context. The key contributions of this paper are as follows:

- 1) *Reflector-Terminal CPD (R-CPD)*: We develop a CPD scheme tailored for reflector terminals within EMLP-CNC. Using the Link Allocation Algorithm based on the Perfect Matching Model (LAA-PMM) [34], we generate an optimal reflector topology (R-Topo). This topology is designed to meet users’ large-volume data communication needs by strategically connecting satellites to GSs based on the number of available reflector terminals and user requirements defined by ground operators.
- 2) *Phased Array Terminal CPD (P-CPD)*: Building on the optimal R-Topo, we design a CPD scheme for phased array terminals. Utilizing the Maximum Weight Matching Algorithm [35], we construct a phased array topology (P-Topo) that addresses the ranging and communication needs of satellites while providing navigation and small-volume data communication services for users. The R-Topo enhances the P-CPD by improving communication efficiency and service capacity.
- 3) *Extensive Simulations and Validation*: We perform comprehensive simulations within the EMLP-CNC framework to validate the proposed CPD schemes. The results demonstrate that the R-CPD and P-CPD are practical and effective for real-world implementation, offering a feasible approach to operationalizing EMLP-CNC. The obtained results provide the first performance benchmark for CPD-based Cislunar networks.

The structure of this paper is organized as follows: Section II reviews the related work, summarizing CPD and Cislunar

infrastructure advancements. Section III details the networking model of EMLP-CNC, including its node architecture and link characteristics. Section IV introduces R-CPD, presenting the algorithm and optimization strategies for reflector topologies (R-Topo). Section V investigates the influence of R-Topo on phased array terminals and proposes P-CPD for phased array topologies (P-Topo). Section VI provides a comprehensive performance analysis of the R-CPD and P-CPD-generated topologies, validating their efficiency through simulations. Finally, Section VII concludes the paper with key findings and future research directions.

II. BACKGROUND

This section provides context and related research on Cislunar Space Networks and Contact Plan Design.

A. Cislunar Space Infrastructures

Cislunar space infrastructure encompasses a comprehensive network of engineering systems strategically deployed in Cislunar space to facilitate resource development and support the expansion of human activity beyond Earth. These infrastructures are designed to deliver critical services, including data communication, positioning, navigation, and timing (PNT), addressing the diverse needs of ground-based and near-Earth users, Cislunar flight operations, lunar surface activities, and deep-space missions. By integrating these capabilities, Cislunar infrastructure aims to ensure robust support for scientific exploration, resource utilization, and the extension of human presence in space.

1) *Actors and Projects*: This collaborative momentum highlights the critical role of such infrastructure in enabling sustained lunar exploration, resource utilization, and the expansion of human presence beyond Earth. The development of Cislunar space infrastructure reflects a growing consensus among the leading spacefaring nations and organizations listed below.

a) *LunaNet (NASA)*: NASA’s LunaNet [6] envisions a scalable lunar communication and navigation architecture that integrates topological configurations, including surface-based and orbiting provider nodes. This initiative aims to support the growing demand for communication and navigation services across manned and unmanned lunar missions.

b) *Moonlight (ESA)*: Similarly, ESA’s Moonlight initiative [36] focuses on establishing the Lunar Communications and Navigation Services system and its associated infrastructure. The program proposes deploying a network of spacecraft around the Moon, enabling comprehensive support for lunar exploration activities while fostering collaboration with European aerospace companies to deploy communication and navigation satellites.

c) *Lunar Navigation Satellite System (JAXA, NASA, and ESA)*: The Japan Aerospace Exploration Agency (JAXA) has introduced the Lunar Navigation Satellite System (LNSS) [37], a constellation modeled after GNSS to provide navigation services and facilitate Earth-Moon communication relay. NASA, ESA, and JAXA are collaborating to establish the first batch

of these lunar network service nodes. This initial network comprises two NASA Lunar Communication Relay Navigation System satellites, one ESA Moonlight Program satellite, and one JAXA LNSS satellite. All operate in circumlunar elliptical frozen orbits to provide continuous communication and navigation services, particularly focused on the Moon's south pole.

d) China Aerospace Science and Technology Corporation (CASC): China Aerospace Science and Technology Corporation (CASC) has proposed a comprehensive Cislunar infrastructure [38], comprising five key components: ground facilities, near-Earth constellations, near-lunar constellations, extended space constellations, and lunar surface facilities. The extended space constellations are of particular interest. These involve deploying satellites at the Earth-Moon libration points, providing uninterrupted, all-space services for users across the Cislunar domain.

2) Libration Points: Due to their unique gravitational and dynamic properties, libration points are pivotal in lunar and deep space exploration. These points enable the stable positioning of satellites relative to the Earth and Moon, making them ideal for constructing advanced navigation and communication systems. The following studies demonstrate the strategic value of libration points for enabling robust, scalable, and autonomous navigation and communication systems critical to the future of Cislunar and deep space missions.

The trajectory design and implementation of four Chinese libration point missions, as detailed in [12], exemplify their importance. These missions include two Sun-Earth libration point missions (CHANG'E-2 and CHANG'E-5) and two lunar libration point missions (CHANG'E-5T1 and Queqiao), which demonstrate China's commitment to leveraging libration points for lunar exploration.

The work in [9] establishes that navigation constellations deployed at libration points can achieve precise orbit determination by relying solely on inter-satellite links. This capability arises from the inherent gravitational asymmetry around these points, eliminating the need for ground-based tracking. Expanding on this, [10] introduces a constellation design methodology tailored to provide high-precision navigation services for Cislunar users, showcasing the practical feasibility of such systems.

Further innovations are discussed in [13], which presents a five-satellite constellation featuring three halo orbit satellites and two distant retrograde orbit (DRO) satellites. This configuration achieves 100% continuous single-fold coverage of the entire lunar surface, underscoring the potential of libration point-based constellations for comprehensive spatial coverage.

The autonomous navigation accuracy achievable through libration point systems is investigated in [11], highlighting using translunar libration point satellites as navigation relays augmented by GPS signals. This integration significantly enhances the precision of lunar exploration trajectories.

Lastly, [14] proposes a low-thrust controller designed for autonomous orbit maintenance of libration point satellites. This controller minimizes fuel consumption by leveraging

autonomous orbit determination results while ensuring long-term orbital stability.

3) Onboard Terminals: Adopting large-aperture reflector antennas on satellites is one of the solutions to meet the growing data demand in space systems [15]. The work in [39] provides the current progress status of large deployable spaceborne reflector antennas and reveals the unique advantages of using high-gain reflector antennas in space telecommunications, earth observation, and space science. Authors in [17] describe the design, ground testing, in-orbit experiments, and a novel in-orbit operation for large deployable reflector antennas. Two large deployable reflector antennas are installed on Engineering Test Satellite VIII for the experiment. [18] briefly introduces the TerreStar satellite: the TerreStar-1 satellite is the world's largest commercial satellite, which communicates with tiny earth terminals and achieves very high antenna gain to receive uplink signals through a large-aperture reflector antenna.

However, mechanically scanned reflector antennas have large inertia and slow steering speeds. Adopting phased array antennas is one of the best approaches to overcoming these challenges. Phased array antennas are characterized by rapid beam scanning and agile beam shaping, among other features. The study in [16] summarizes the development process of spaceborne active phased array antennas, analyzing the structural forms, performance requirements, and application scenarios of spaceborne active phased array antennas. [16] also points out that although large-aperture, high-power phased array antennas can also bring high gain and data rates, their design costs, power consumption, and cooling requirements significantly increase. Moreover, the high current required for high power poses considerable risks for space applications.

Phased array antennas are primarily used for inter-satellite ranging in navigation constellations and do not handle much communication traffic. Therefore, large-aperture, high-power phased array antennas are not needed in navigation constellations; instead, phased array antennas with aperture and power that meet the ranging requirements and stable performance should be used.

4) Spatial Users: The research and engineering community has been motivated by the deployment of satellites at the Earth-Moon libration points to build a robust Cislunar infrastructure and the leveraging of inter-satellite links for navigation and communication services for spatial users.

Currently, navigation for most spatial users relies predominantly on ground-based measurements. For instance, the Chang'E-4 (CE-4) mission demonstrated a positional precision of better than 100 meters by leveraging ground-based ranging measurements and Very Long Baseline Interferometry (VLBI) data during orbit determination [40]. However, as the distance between the spacecraft and Earth increases, the geometric configuration of ground-based measurement systems deteriorates significantly, leading to reduced accuracy and reliability.

To address these limitations, autonomous orbit determination through space-based measurements has been proposed. Among the technologies explored are inter-satellite ranging

and GNSS sidelobe signal positioning. Inter-satellite ranging enables precise orbit determination without relying on ground stations, making it particularly suitable for deep space missions. Conversely, while promising, GNSS sidelobe signal navigation faces challenges such as low signal energy, limited visibility of satellites, and a poor precision factor, restricting its utility [41].

Deploying satellites near the Lagrange points offers an effective alternative for navigation. The study in [42] demonstrated that such constellations can achieve navigation and positioning accuracy better than tens of meters, even for spacecraft operating far from Earth. This is enabled by the establishment of a space-time reference system within Earth-Moon space, which utilizes inter-satellite ranging to achieve high-precision orbit determination and navigation.

While these studies show the relevance of, the key challenge lies in efficiently scheduling these inter-satellite links. This task necessitates the development of advanced Contact Plan Design (CPD) schemes to optimize link allocation under the unique constraints of the Cislunar environment.

B. Contact Plan Design

A contact is an opportunity to establish a temporary communication link between two nodes when physical requirements, such as antenna alignment and sufficient received power, are met. Such feasible contacts within a network during a specific interval constitute the contact topology. From this, a subset of selected contacts forms the contact plan, which determines the actual links to be implemented, considering constraints such as interference, power, and resource limitations. The process of determining this optimal subset is called Contact Plan Design (CPD) [19].

1) *CPD for Navigation Systems*: For GNSS (Global Navigation Satellite Systems), the primary objectives of CPD include maximizing ranging opportunities, achieving frequent and diverse observations, and minimizing end-to-end data delivery delay. CPD research for GNSS can be broadly categorized based on the methodologies employed:

- 1) *Linear Programming*: Studies such as [23] optimize communication performance while adhering to GNSS-specific constraints, such as consistent ranging. Similarly, [25] extends polling mechanisms to ground-satellite links, aiming to minimize the average data delivery delay from satellites to ground stations.
- 2) *Specific Rule-Based Approaches*: The work in [30] introduces a grouping-based strategy for improving CPD efficiency, optimizing both ranging observations and low-delay communications. Authors in [27] outline a three-step link scheduling method that combines a genetic algorithm with prioritized downlink routes. Additionally, [31] enhances link allocation with an adaptive topology optimization algorithm that leverages prior knowledge for iterative improvement.
- 3) *Matching Algorithms*: A distributed CPD approach is first proposed in [24], while [26] employs a hybrid of bipartite and general matching to improve inter-satellite

ranging and communication performance. In [33], links are classified into four categories with tailored weight adjustments to enhance CPD outcomes.

- 4) *Heuristic Algorithms*: The work in [29] formulates CPD as a constraint optimization problem and solves it using simulated annealing, while [28] combines genetic algorithms with the Blossom algorithm to achieve optimal matching for satellite sequences. In [32], a double-loop optimization algorithm addresses complex scheduling challenges in CPD.

2) *CPD for Communication Systems*: The CPD objective often shifts towards minimizing end-to-end transmission delay and maximizing throughput for communication constellations. Unlike GNSS, communication constellations frequently utilize relatively static topologies with satellites equipped with multiple inter-satellite link (ISL) terminals. Early constellations, such as Iridium [43], adopt a fixed topology where each satellite establishes links with adjacent satellites in the same orbit and neighboring orbital planes. In [44], a repeating “motif” pattern is introduced for ISLs, enhancing network capacity with slight sacrifices in delay. However, this approach avoids establishing links between satellites moving in opposite directions, limiting flexibility. Dynamic optimization of inter-plane links is addressed in [45], which proposes inter-plane links to reduce delays in extensive low-Earth orbit constellations. Expanding on this, [46] introduces a multi-agent deep reinforcement learning-based framework for dynamic ISL planning, optimizing total throughput and reducing switching rates.

Despite these advancements, existing CPD efforts primarily focus on optimizing satellite-to-satellite ranging and communication, neglecting the service requirements of spatial users. To bridge this gap, this paper investigates a CPD framework tailored for satellites deployed at Earth-Moon libration points equipped with reflectors and phased array terminals. This framework simultaneously addresses satellites’ ranging and communication needs while prioritizing user services through effective scheduling of RLs and PLs. By integrating these capabilities, this work establishes a robust CPD strategy to serve both system—and user-level demands.

III. SYSTEM MODEL

The EMLP-CNC model is designed to support spatial users and inter-satellite communications in the Cislunar environment. In this system, each satellite is equipped with multiple reflector terminals and a single-phased array terminal, providing dual-mode capabilities to handle diverse communication and navigation demands. Spatial users are equipped with one reflector terminal and one phased array terminal. This dual-terminal architecture ensures satellites and users can adapt dynamically to the evolving network topology and mission requirements. At the same time, ground stations (GSs) can accommodate an arbitrary number of reflector terminals to facilitate high-capacity data links.

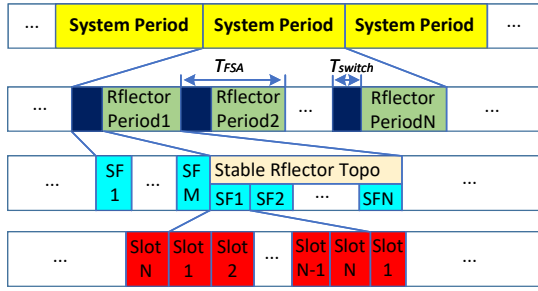


Fig. 2. EMLP-CNC topology model

A. Topology Model

The EMLP-CNC topology model integrates different operational schemes for phased array links (PLs) and reflector links (RLs) to accommodate their distinct characteristics. PLs leverage Concurrent Spatial Time Division Duplexing (CSTDD) for efficient and flexible link utilization, while RLs rely on a Finite State Automaton (FSA) scheme to minimize frequent link switching and maintain stability [47].

CSTDD is a communication technique that enables multiple directional links to operate simultaneously by leveraging spatial separation while still adhering to time-division multiplexing for duplex communication. In the FSA scheme, the network operates in discrete states, with static visibility between nodes. Two nodes are considered visible within a state if and only if they maintain uninterrupted visibility throughout the state duration. This approach ensures that RL topology (R-Topo) remains stable during each FSA state, aligning with the mechanical constraints of RLs.

To integrate CSTDD and FSA effectively within EMLP-CNC [48], the operational timeline is divided into equal-length reflector periods, as depicted in Fig. 2. Each reflector period begins with a reserved interval dedicated to RL switching. During this interval, only non-switching RLs and PLs are operational. Once this phase concludes, the R-Topo stabilizes for the remainder of the reflector period, enabling reliable large-volume data transfer.

Reflector periods are further segmented into superframes, which serve as the scheduling units for phased array-based Contact Plan Design (P-CPD). Each superframe is divided into multiple time slots, representing the unit duration required to establish and maintain a PL. Within each slot, satellites utilizing PLs execute tasks such as ranging and data exchange [49]. This hierarchical time-division structure optimally balances RLs' stable but slower dynamics with PLs' agility and rapid switching capabilities, enabling seamless operation of the EMLP-CNC network.

B. Link Model

The network supports various types of links, as illustrated in Fig. 3 and enumerated in Table II: reflector links (RL) between satellites, phased array links (PL) between satellites, RLs between satellites and users, PLs between satellites and users, and RLs between satellites and ground stations (GS).

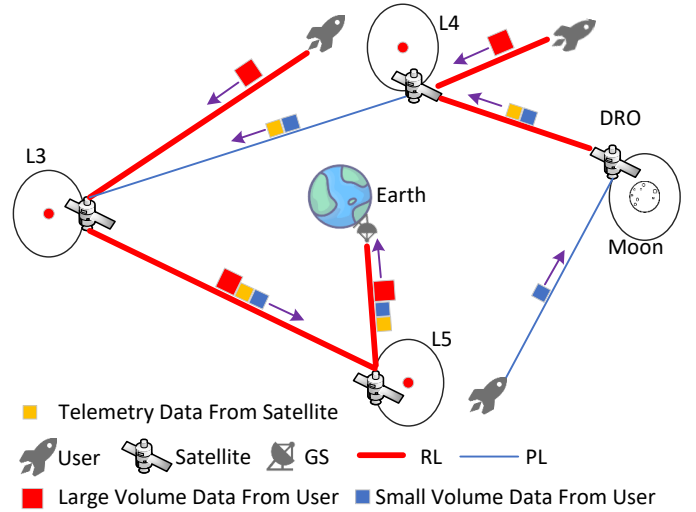


Fig. 3. EMLP-CNC link and traffic models.

TABLE II
TYPES OF LINKS IN EMLP-CNC

Link Type	Description
RL(Sat,Sat)	Reflector links between satellites.
PL(Sat,Sat)	Phased array links between satellites.
RL(Sat,User)	Reflector links between satellites and users.
PL(Sat,User)	Phased array links between satellites and users.
RL(Sat,GS)	Reflector links between satellites and GSs.

Users in this system cannot establish direct links with one another or ground stations; instead, all data must be relayed to ground stations via satellites.

The system distinguishes the roles of these links based on their technical capabilities. PLs are suited for small-volume data transfer, such as telemetry or phased array user communications. At the same time, RLs can support both large-volume and small-volume data, fulfilling the high-throughput demands of reflector users. Additionally, PLs are employed for inter-satellite ranging, enabling precise navigation services for phased array users.

RLs and PLs work to fulfill the system's communication and navigation functions. Large-volume data generated by reflector users is exclusively transmitted through the evolving R-Topo over multiple reflector periods. In contrast, small-volume data generated by phased array users or satellites is delivered through the evolving P-Topo across multiple time slots, augmented by the R-Topo within the current reflector period.

Users are assumed to have only access capabilities, meaning they transmit their data to a connected satellite as soon as a link is established. Satellites then compute end-to-end paths using a routing algorithm [50] within a store-and-forward network, adhering to the principles of Delay/Disruption Tolerant Networking (DTN) [19], [51]. This collaborative framework ensures efficient management of diverse traffic requirements within the EMLP-CNC.

TABLE III
DEFINITION OF IMPORTANT NOTATION

symbol	definition
L_G	The desired number of RL(Sat, GS)s that the ground operator aims to build in the optimal R-Topo
U_R	The reflector user requirements set by the ground operators
$ U_R $	The number of reflector users in U_R
\vec{w}	Weight coefficients in the objective of R-Topo optimization
U_P	The phased array user requirements set by the ground operators
$ U_P $	The number of phased array users in U_R
\vec{C}	In P-CPD, the ranging constant, communication constant, and user service constant that influence the maximum weight matching

C. Traffic Model

The primary traffic in EMLP-CNC comprises data transmitted to ground stations (to-GS traffic), including large-volume data, such as user-generated high-throughput communication, and small-volume data, such as telemetry messages originating from satellites. Secondary traffic includes navigation messages exchanged between satellites and telecommands sent from ground stations to satellites.

IV. R-CPD METHOD

The R-Topo is the foundational framework for transferring large-volume data from reflector users to ground stations. This section introduces the mathematical model for optimizing the R-Topo and explains how to determine the optimal configuration using LAA-PMM [34], executed iteratively across multiple scenarios. Table III lists important notation in this paper.

In the proposed model, nodes are denoted by their type and identifier: satellite (S), user (U), and ground station (G). The visibility between reflector terminals during each reflector period is represented as an undirected graph $G_R(V, E)$. The vertex set V includes all satellites, users, and ground stations, partitioned into subsets V^s , V^u , and V^g , representing satellites, users, and ground stations, respectively. Their cardinalities are given by $N^s = |V^s|$, $N^u = |V^u|$, and $N^g = |V^g|$, with the total set defined as $V = V^s \cup V^u \cup V^g$. The edge set E represents potential reflector links (RLs) between nodes with mutual visibility.

The optimized R-Topo, denoted as $H_R(V, E)$, is a sub-graph of $G_R(V, E)$, containing the subset of nodes and edges involved in established RLs during the given period. This topology is derived by solving the R-CPD problem, ensuring the network configuration satisfies the system's traffic and connectivity requirements. Figure 4(a) illustrates an example of $G_R(V, E)$ for a specific reflector period, while Figure 4(b) displays the corresponding optimized $H_R(V, E)$, highlighting the active nodes and RLs selected for that period.

In the network model, each node v in the graph $G_R(V, E)$ is equipped with $f(v)$ reflector terminals, representing its

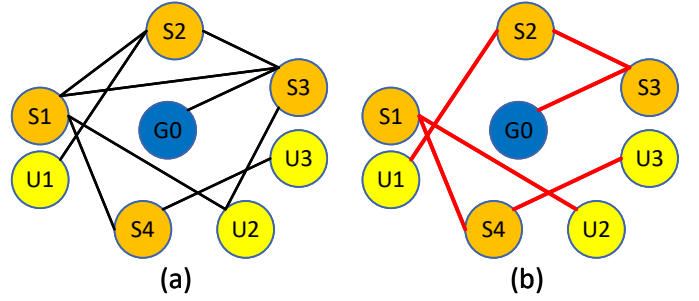


Fig. 4. An example of R-CPD

maximum capacity to establish RLs. Each established RL(x, y) utilizes one reflector terminal at participating nodes x and y . The parameter $g(v)$ quantifies the visible edges between node v and other nodes in $G_R(V, E)$. For example, in Fig. 4(a), node U2 is visible to nodes S1 and S3, resulting in $g(U2) = 2$.

The variable $d(v)$ denotes the number of RLs established at node v in the optimized topology $H_R(V, E)$. To ensure feasibility, $d(v)$ must satisfy two key constraints:

$$d(v) \leq f(v) \quad (1)$$

$$d(v) \leq g(v) \quad (2)$$

The first constraint, (1), ensures that the number of established RLs does not exceed the physical capacity of the reflector terminals at node v . The second constraint, (2), guarantees that $d(v)$ is limited by the visibility of node v to other nodes in the graph, as defined by $g(v)$. These constraints collectively regulate the allocation of RLs in $H_R(V, E)$ to maintain network consistency and optimal performance.

A. Objectives

The performance of the R-Topo is evaluated using a weighted combination of four optimization objectives:

O1: Stability: Given the mechanical constraints of reflector terminals, R-CPD aims to minimize terminal switching during the transition from the previous reflector period's optimal R-Topo, $H_R(V, E)_{pre}$, to the current one, $H_R(V, E)$. The stability objective function for satellites is defined as:

$$f_1 = \frac{L_{stable}}{L_{pre}} \quad (3)$$

Here, L_{stable} represents the total number of RLs that remain unchanged during the transition, while L_{pre} denotes the total number of RLs in $H_R(V, E)_{pre}$.

O2: Connectivity between satellites and GSs: A satellite x is considered a directly grounded satellite (DG-Sat) if there exists an RL($Sat\ x, GS$), indicating a direct connection to a ground station. A satellite z is classified as an indirectly grounded satellite (IDG-Sat) if it is not directly connected to GSs but its reflector terminal establishes a link with a DG-Sat x . Both DG-Sats and IDG-Sats can transfer data to GSs within the reflector period and are collectively referred to as grounded satellites (G-Sats). Satellites that do not belong to the

G-Sats group are termed ungrounded satellites (UG-Sats). For instance, in Fig. 4(b), $S3$ is a DG-Sat, $S2$ is an IDG-Sat, while $S1$ and $S4$ are UG-Sats. The connectivity between satellites and GSs improves as the number of G-Sats increases. Let the total number of G-Sats in $H_R(V, E)$ be N^{gs} , with all G-Sats forming the set V^{gs} . The objective function for evaluating the connectivity between satellites and GSs is defined as:

$$f_2 = \frac{N^{gs}}{N^s} \quad (4)$$

This function represents the proportion of G-Sats among all satellites, emphasizing the network's grounding capability.

O3: Connectivity among satellites: The connectivity among satellites improves with an increasing number of RLS between satellites. In Fig. 4(b), examples of such links include $RL(S1, S4)$ and $RL(S2, S3)$, both of which are classified as $RL(\text{Sat}, \text{Sat})$. Assume that the total number of $RL(\text{Sat}, \text{Sat})$ links in $H_R(V, E)$ is L^{ss} . The objective function for evaluating the connectivity among satellites is defined as:

$$f_3 = \frac{L^{ss}}{L_{max}^{ss}}. \quad (5)$$

Here, $L_{max}^{ss} = \frac{N^s(N^s-1)}{2}$ represents the maximum possible number of RLS between satellites in a fully connected topology. This function highlights the proportion of established inter-satellite links relative to the maximum possible number, thereby measuring the network's satellite-to-satellite connectivity.

O4: Service Capability for Users: The service capability for users is determined by the availability of RLS connecting users to GSs. If an $RL(\text{G-Sat } y, \text{User } x)$ exists, the data of User x can be sent to GSs within the current period, classifying x as a real-time (RT) user. Conversely, if an $RL(\text{UG-Sat } y, \text{User } x)$ exists, User x 's data cannot be sent to GSs within the period, making x a non-real-time (NRT) user. For example, in Fig. 4(b), $U1$ is classified as an RT user, while $U2$ and $U3$ are NRT users. Assuming that $H_R(V, E)$ includes N^{rt} RT users and N^{nrt} NRT users, the objective function for evaluating the service capability for users is defined as:

$$f_4 = \frac{N^{rt} + \alpha N^{nrt}}{N^u}. \quad (6)$$

In this paper, $\alpha = 0.7$, which biases R-CPD towards prioritizing RT users.

O1-4: Weighted global objective: Based on the above discussion, the R-CPD for a reflector period can be formulated as follows: The goal is to identify a subgraph $H_R(V, E)$ within $G_R(V, E)$ that satisfies the constraints (1), (2) and maximizes the objective function:

$$\max F = w_1 f_1 + w_2 f_2 + w_3 f_3 + w_4 f_4. \quad (7)$$

This formulation encapsulates the optimization of stability, connectivity to GSs, inter-satellite connectivity, and user service capability in a single weighted objective function.

B. Algorithm

The R-CPD process begins with visibility preprocessing, followed by executing the Link Allocation Algorithm based on the Perfect Matching Model (LAA-PMM) [34] multiple times to determine the optimal R-Topo. LAA-PMM transforms the original link allocation problem into a perfect matching problem. It enables terminal allocation to create a topology where all terminals are utilized to establish links, leaving no terminals idle.

An example of this process is illustrated in Fig. 4. In the scenario depicted in Fig. 4(a), each satellite has two reflector terminals, while users and GSs each have one terminal. Applying LAA-PMM to Fig. 4(a) produces the resulting topology shown in Fig. 4(b). In this topology, all terminals across all nodes are fully utilized to establish RLS, ensuring no terminals remain idle. Fig. 5 illustrates the preprocessing steps, with Fig. 5(a) showing the original graph $G_R(V, E)$ before preprocessing and Fig. 5(f) depicting the resulting graph $G_R^*(V, E)$ after preprocessing. The remainder of this subsection will formally describe the LAA-PMM process at the core of the R-CPD method.

1) *Preprocess:* Before applying LAA-PMM, the parameters L_G and U_R must be set to preprocess $G_R(V, E)$ into $G_R^*(V, E)$. Here, L_G represents the desired number of $RL(\text{Sat}, \text{GS})$ s that the ground operator aims to include in $H_R(V, E)$. U_R represents the reflector user requirements set by the ground operators. Specifically, U_R is defined as $U_R = [(User_1, True/False), \dots, (User_n, True/False)]$, where $(User_n, True)$ signifies that $User_n$ wishes to be a RT user in $H_R(V, E)$, while $(User_n, False)$ indicates that $User_n$ can be a non-RT user without a mandatory need for real-time service. The preprocessing involves specific steps to modify the graph to meet the requirements set by L_G and U_R :

- a) Users cannot directly establish links with other users or GSs. Therefore, visible edges between users and other users and between users and GSs should be removed. Fig. 5(a) to Fig. 5(b) correspond to this step, denoted as step (a).
- b) Next, all GS nodes are merged into a logical GS node, denoted as $G0$. The visibility between $G0$ and satellites is the union of the visibility sets between all individual GS nodes and satellites before merging. This abstraction focuses on whether satellites establish RLS with GSs rather than specifying which particular GS they connect to. The value of L_G determines the number of reflector terminals assigned to $G0$, i.e., $f(G0) = L_G$. Fig. 5(b) to Fig. 5(c) illustrate step (b), where nodes $G1$ and $G2$ are merged into $G0$. For input $L_G = 3$, we obtain $f(G0) = 3$.
- c) Not all users have communication requirements in every reflector period. Thus, only users listed in U_R are retained in the graph. Fig. 5(c) to Fig. 5(d) correspond to step (c), where $U_R = [(U1, True), (U3, False), (U4, False)]$. As a result, only users $U1$, $U3$, and $U4$ are kept, while all other users are removed.

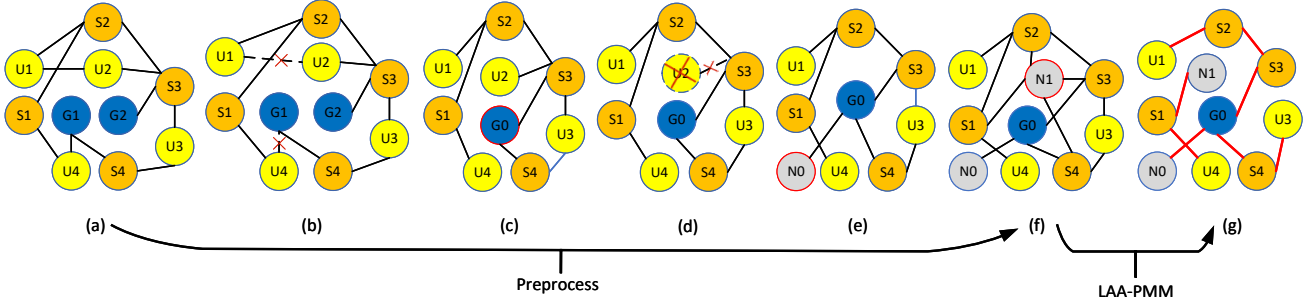


Fig. 5. LAA-PMM preprocessing example.

- d) LAA-PMM strives to avoid idle terminals, requiring that every node v in $G_R(V, E)$ satisfies:

$$g(v) \geq f(v) \quad (8)$$

To ensure condition (8), virtual nodes with no practical significance are introduced, denoted as type N . For each node v that does not satisfy (8), virtual nodes are added such that the total visibility matches the terminal capacity. Specifically, $f(v) - g(v)$ virtual nodes are added, each equipped with one reflector terminal visible only to v . Fig. 5(d) to Fig. 5(e) correspond to step (d). For example, since $f(G0) = 3$ and $g(G0) = 2$, a virtual node $N0$ is introduced, visible only to $G0$, ensuring that $f(G0) = g(G0) = 3$.

- e) To establish a link, two terminals are required. Thus, for the graph $G_R(V, E)$ (including virtual nodes added in step (d)), the sum of terminal numbers across all nodes must be even to avoid idle terminals. If the sum is odd, an additional virtual node is introduced. This virtual node is equipped with one reflector terminal and is visible to all satellites, ensuring the total number of terminals becomes even. Fig. 5(e) to Fig. 5(f) illustrate this process, corresponding to step (e). In Fig. 5(e), since the terminal sum is odd, a virtual node $N1$ with one reflector terminal and visibility to all satellites is added to make the sum even.

At the end of the preprocessing stage, the original graph $G_R(V, E)$ is transformed into $G_R^*(V, E)$. In this processed graph, all nodes satisfy the constraint (8), ensuring each node has sufficient visibility to establish the required links. Additionally, the sum of terminal numbers across all nodes in $G_R^*(V, E)$ is even, avoiding idle terminals. Users and GSs maintain visible edges exclusively with satellites, and only the users specified in U_R are retained in $G_R^*(V, E)$.

2) *Execution*: Applying LAA-PMM to $G_R^*(V, E)$ results in $H_R^*(V, E)$, where all terminals of all nodes are utilized for link establishment due to the nature of LAA-PMM.

Fig. 5(g) illustrates the outcome of applying LAA-PMM to the preprocessed graph shown in Fig. 5(f). When virtual nodes are treated as normal nodes, the resulting topology ensures that all terminals are used to establish RLs, leaving no idle terminals. However, virtual nodes hold no practical

significance. For instance, one terminal of $G0$ is connected to the virtual node $N0$, indicating an idle reflector terminal for $G0$. This occurs because $G0$ has three reflector terminals but is only visible to two satellites, allowing for a maximum of two RLs. Similarly, one reflector terminal of satellite $S1$ remains idle in this scenario.

Without considering virtual nodes, users in $G_R^*(V, E)$ are only connected to satellites, ensuring that LAA-PMM establishes links between users and satellites in $H_R^*(V, E)$. Similarly, GSs are guaranteed to form links with satellites. The set U_R determines which users are retained in $G_R^*(V, E)$ and, consequently, influences the number of $RL(\text{Sat}, \text{User})$ s in $H_R^*(V, E)$. Likewise, L_G specifies $f(G0)$, directly affecting the number of $RL(\text{Sat}, \text{GS})$ s. By configuring U_R and L_G , ground operators can roughly control the service capacity and the connectivity between satellites and GSs in $H_R^*(V, E)$. When $|U_R|$ and L_G are small, more reflector terminals are available for $RL(\text{Sat}, \text{Sat})$ s, enhancing satellite connectivity.

Given the inherent randomness of LAA-PMM, executing LAA-PMM multiple times on the same $G_R^*(V, E)$ may yield different $H_R^*(V, E)$. Among these outcomes, the $H_R^*(V, E)$ that satisfies U_R and maximizes the objective function F is selected as the optimal R-Topo $H_R(V, E)$. The entire R-CPD process for a reflector period is outlined in Algorithm 1. In line 3, $G_R(V, E)$ is obtained based on the visibility analysis conducted using AGI STK. The default value for NF is set to 20. Define $\vec{w} = [w_1, w_2, w_3, w_4]$.

V. P-CPD METHOD

Each satellite in EMLP-CNC is equipped with a single-phased-array terminal [16]. The P-Topo is formed as pairs of nodes and can be planned using matching algorithms from graph theory [35]. In an undirected graph, matching represents a set of edges where no two edges share a common vertex, and the maximum weight matching corresponds to the matching with the largest sum of edge weights [52]. Building upon the optimal R-Topo, this section proposes a heuristic algorithm for P-CPD in EMLP-CNC, utilizing the maximum weight matching approach.

A. The Impact of R-Topo on P-CPD

Previous P-CPD studies categorized satellites into anchor and non-anchor satellites based on their ability to establish

Algorithm 1 R-CPD in a reflector period

Input: Constellation parameters, $f(v)$, NF , $H_R(V, E)_{pre}$,

U_R , L_G , \vec{w}

Output: $H_R(V, E)$ which satisfies U_R and get max F

- 1: **Begin**
 - 2: $count=1$
 - 3: Generate the possible graph $G_R(V, E)$
 - 4: Preprocess $G_R(V, E)$ to $G_R^*(V, E)$
 - 5: **while** $count \leq NF$ **do**
 - 6: $H_R^*(V, E)=LAA-PMM(G_R^*(V, E))$
 - 7: Get the F of $H_R^*(V, E)$, and $count++$
 - 8: **end while**
 - 9: Get the $H_R(V, E)$ which satisfies U_R with max F among all NF $H_R^*(V, E)$ instances
 - 10: **End**
-

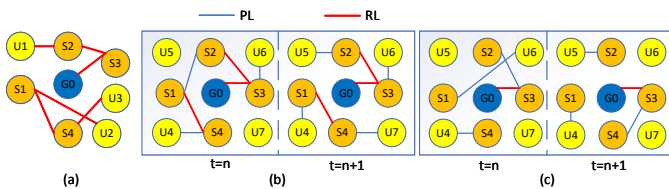


Fig. 6. An example of the impact of R-Topo on P-CPD

links with GSs [23]–[27]. Anchor satellites can send data to GSs directly in the current time slot. In contrast, non-anchor satellites rely on establishing PLs with anchor satellites to relay their data to GSs via the anchor satellites. Notably, the data considered in P-CPD pertains exclusively to small-volume data transmitted through PLs. Based on the structure of R-Topo, P-CPD introduces two significant differences from previous approaches:

- 1) Consistent with earlier definitions, DG-Sats serve as anchor satellites, while IDG-Sats act as non-anchor satellites. However, the presence of RL(DG-Sat, IDG-Sat)s allows IDG-Sats to relay their data to DG-Sats, which subsequently transmit the data to GSs. This eliminates the necessity for PL(DG-Sat, IDG-Sat)s from a communication standpoint.
- 2) If RL(UG-Sat, UG-Sat)s exist, all connected UG-Sats form a set denoted as V_m^{ugs} , where $m \in \mathbb{N}^+$ and m represents the m -th UG-Sats set. An isolated UG-Sat forms its own set. If any UG-Sat within a UG-Sats set establishes a PL with any G-Sat, the entire UG-Sats set can send data to GSs.

Fig. 6 illustrates the advantages of performing P-CPD based on R-Topo. In Fig. 6(a), the obtained $H_R(V, E)$ is depicted. Fig. 6(b) demonstrates the results of P-CPD over two-time slots based on $H_R(V, E)$ (excluding RL(Sat, User)s). At the $t = n$ slot, UG-Sat S1 established a PL with G-Sat S2, enabling all UG-Sats in the UG-Sats set $V_1^{ugs} = [S1, S4]$ to transmit data to GSs during this time slot. Across two time slots, P-CPD successfully transmitted data to GSs for all satellites and served six phased array users. In contrast,

Fig. 6(c) illustrates the results of P-CPD over two-time slots without considering $H_R(V, E)$ (but retaining RL(Sat, GS)s). Here, P-CPD only succeeded in transmitting data to GSs for S2, S3, and S4, while serving just four users. A comparison between Fig. 6(b) and Fig. 6(c) highlights two key benefits brought by $H_R(V, E)$ to P-CPD:

- 1) R-Topo enhances the connectivity among satellites, enabling P-CPD to transmit data to GSs for all satellites with fewer time slot resources, thereby reducing the overall to-GS delay.
- 2) R-Topo provides P-CPD with richer time slot resources for serving users, thereby expanding the service capacity of satellites for phased array users.

Furthermore, the mechanical nature of RLs causes the transition from $H_R(V, E)_{pre}$ to $H_R(V, E)$ to require a significant amount of time, during which only non-switching RLs exist. This transition period is referred to as the dynamic phase of R-Topo. Once all RLs are switched, the R-Topo remains unchanged for the remainder of the reflector period, referred to as the stable phase of R-Topo. The UG-Sats set V_m^{ugs} and the G-Sats set V^{gs} during the dynamic phase of R-Topo differ from those during the stable phase. Therefore, P-CPD within a single reflector period is divided into two stages: the P-CPD in the dynamic phase of R-Topo and the P-CPD in the stable phase of R-Topo.

B. Mathematic Model and Algorithm

1) *Basic Model:* Model the visibility between nodes' phased array terminals in each reflector period as an undirected graph $G_P(V, E, W)$, where V is the set of all satellites and users. E is the set of visible edges between all nodes' phased array terminals, i.e., the set of possible PLs. W is the weight set of all visible edges. The visible edges between satellites and users, satellites and satellites, UG-Sats and UG-Sats, G-Sats and G-Sats, UG-Sats and G-Sats is denoted by $\varepsilon^{s-u}, \varepsilon^{s-s}, \varepsilon^{ugs-ugs}, \varepsilon^{gs-gs}, \varepsilon^{ugs-gs}$ respectively.

Similar to the preprocessing of R-CPD, according to the phased array user needs U_P set by ground operators, retaining only those users with PLs needs in the current period in $G_P(V, E, W)$. $U_P = [(x, L_x^u), \dots, (z, L_z^u)]$, where (x, L_x^u) represents that user x expects satellites to provide L_x^u PLs in a superframe for x . This paper does not differentiate whether satellites use PLs to provide small-volume data communication services or navigation services for users; it only concerns the number of PLs satellites provide for users. Additionally, remove the edges between users in $G_P(V, E, W)$ to avoid PLs between users.

2) *Weights Assignment for Edges:* To satisfy U_P , define the weight $w_{i,j,t}^u$ of the $e_{i,j}$ between any user i and any satellite j in $G_P(V, E, W)$ at each time slot as follows:

$$w_{i,j,t}^u = \begin{cases} (L_i^u - L_{i,j,t}) \cdot C_1, & \sum_{k \in V^s} L_{i,k,t} < L_i^u \\ 0, & \sum_{k \in V^s} L_{i,k,t} \geq L_i^u \end{cases} \quad \forall e_{i,j} \in \varepsilon^{s-u}, 1 \leq t \leq T \quad (9)$$

C_1 is the service weight constant. T is the number of time slots in a superframe. $L_{i,j,t}$ represents the number of times that satellite j provides link establishment for user i in the previous $t-1$ time slots. When the total number of all satellites for user i $\sum_{k \in V^s} L_{i,k,t}$ is less than L_i^u , the larger $L_{i,j,t}$, the smaller $w_{i,j,t}^u$. If there exists a satellite p such that $L_{i,p,t} < L_{i,j,t}$, then $w_{i,p,t}^u > w_{i,j,t}^u$, the maximum weight matching algorithm will preferentially use satellite p to provide PLs for user i . This allows users to preferentially connect with satellites that have provided fewer PLs, thereby achieving more uniform connections with all satellites, which can improve navigation performance for users. When $\sum_{k \in V^s} L_{i,k,t} \geq L_i^u$, satellites have already met the user's needs, set $w_{i,j,t}^u = 0$, and maximum weight matching algorithm will no longer allow satellites to provide PLs for user i .

To optimize the to-GS delay and meet the ranging needs between satellites, the weight of the edge between any satellite i and other satellite j in $G_P(V, E, W)$ is defined as follows for each time slot:

$$w_{i,j,t} = w_{i,j,t}^c + w_{i,j,t}^r, \quad \forall e_{i,j} \in \varepsilon^{s-s}, 1 \leq t \leq T \quad (10)$$

Wherein the first part $w_{i,j,t}^c$ reflects the contribution degree of planning this edge to communication performance in the current time slot. The second part $w_{i,j,t}^r$ reflects the contribution degree of planning this edge to ranging performance in the current time slot.

In specific, the first part of (10), $w_{i,j,t}^c$, can be given as:

$$w_{i,j,t}^c = \begin{cases} I(i,t) * C_2, & i \in V_m^{ugs}, j \in V^{gs}, \text{if } i = S(V_m^{ugs}) \\ 0, & i \in V_m^{ugs}, j \in V^{gs}, \text{if } i \neq S(V_m^{ugs}) \\ 0, & \forall e_{i,j} \in \varepsilon^{gs-gs} \\ 0, & \forall e_{i,j} \in \varepsilon^{ugs-ugs} \end{cases} \quad 1 \leq t \leq T \quad (11)$$

where $I(i,t)$ represents the grounding potential of the UG-Sat i at the t -th time slot, defining the result of P-CPD for the t -th time slot as the matching result M_t , then:

$$I(i,t) = \begin{cases} 1, & t = 1 \\ 1, & ((\exists e_{x,y} \in \varepsilon^{ugs-gs} \cap M_{t-1}) \text{ and } (x,i \in V_m^{ugs})) \\ I(i,t-1) + 1, & \text{others} \end{cases} \quad 1 \leq t \leq T \quad (12)$$

(12) signifies that for an UG-Sat i , its grounding potential is initialized to 1 in the first time slot. If, in M_{t-1} , there exists a UG-Sat x in the UG-Sats set V_m^{ugs} which i belongs to that has established a PL with any G-Sat y , then the grounding potentials of all UG-Sats in V_m^{ugs} , including UG-Sat i 's, are set to 1. Otherwise, UG-Sat i 's grounding potential equals the grounding potential of the previous time slot plus one. If set V_m^{ugs} does not establish any PL with G-Sats across several consecutive time slots. The grounding potentials of all UG-Sats in this set will increase, thereby providing more opportunities for these UG-Sats to be linked with G-Sats in subsequent matches.

In (11), $S(V_m^{ugs})$ represents a randomly selected UG-Sats from V_m^{ugs} . We only allocate communication weight to the

edges between the selected UG-Sat and G-Sats; the size of the communication weight is the product of the grounding potential of the UG-Sat and the communication constant C_2 . For other UG-Sats in V_m^{ugs} that have not been selected, we do not assign communication weight. Compared to allocating communication weight to every edge connecting each UG-Sat with G-Sats, this method allows V_m^{ugs} to transmit data to GSs by establishing just one PL with G-Sats, enabling satellites to have more time slot resources available for serving users. Any edge between UG-Sats or between G-Sats carries zero communication weight because such edges do not contribute to communication.

The second part of (10), $w_{i,j,t}^r$, can be expressed as:

$$w_{i,j,t}^r = \begin{cases} C_3, & \forall e_{i,j} \in \varepsilon^{s-s}, L_{i,j,t} = 0 \\ 0, & \forall e_{i,j} \in \varepsilon^{s-s}, L_{i,j,t} > 0 \\ \forall e_{i,j} \in \varepsilon^{s-u}, 1 \leq t \leq T \end{cases} \quad (13)$$

$L_{i,j,t}$ denotes the number of times satellite i and satellite j have established links during the previous $t-1$ time slots. If $L_{i,j,t} > 0$, meaning that i and j have already established PLs in the preceding time slots, repeated link establishment offers no significant benefit to ranging, so we set $w_{i,j,t}^r$ to 0. In this paper, we set $C_3 \gg C_1$ and $C_3 \gg C_2$, which ensures that maximum-weight matching algorithm prioritizes planning for ranging time slots. This setup guarantees that each satellite will establish PLs with all other visible satellites at least once, thus obtaining diversified ranging data [29].

3) *A Heuristic Based on Maximum Weight Matching:*

Algorithm 2 illustrates the process of P-CPD based on maximum weight matching. For the k -th reflector period, let $H_P(V, E) = (M_1, M_2, \dots, M_T)$ denote the result in a superframe over T time slots. Define $\vec{C} = [C_1, C_2, C_3]$.

Algorithm 2 P-CPD based on maximum weight matching

Input: Constellation parameters, number of time slots T , All V_m^{ugs} based on $H_R(V, E)$, V^{gs} based on $H_R(V, E)$, \vec{C} , U_P

Output: $H_P(V, E)$

1: **Begin**

2: $t=1$

3: Generate the graph $G_P(V, E, W)$ according to U_P

4: **while** $t \leq T$ **do**

5: Set weight for edges in $G_P(V, E, W)$ according to (9)-(13)

6: Compute the maximum matching

7: According to the matching result M_t , obtain the scheduled topology in the t -th time slot

8: $t=t+1$

9: **end while**

10: Construct $H_P(V, E)$ from (M_1, M_2, \dots, M_T)

11: **End**

VI. EVALUATION

This section evaluates the performance of R-Topo and P-Topo under varying parameters. For R-Topo, the delay is

TABLE IV
BASIC PARAMETERS IN THE SIMULATION

Simulation Duration	30 days
Length of a Reflector Period	30 min
Length of Dynamic Phase of R-Topo	5 min
Length of a Superframe	5 min
Length of a Time Slot	10 s
RL Pointing Range	75°
PL Pointing Range	75°
GS Pointing Range	85°

TABLE V
GS LOCATIONS

GSs	Description
Jiamusi	(46.8°N, 130.3°E)
Kashi	(39.47°N, 75.99°E)
SanYa	(18.23°N, 109.02°E)

quantified as the number of reflector periods (30 minutes) required to transmit large-volume data to GSs. For P-Topo, delay is defined as the number of time slots (10 seconds) required to transmit small-volume data to GSs. Given that the durations of reflector periods and time slots significantly exceed data propagation (typically in the order of 1 second in cislunar space) and transmission delays (typically in the order of milliseconds), this work excludes the latter two types of delays from consideration [27].

The simulation adopts the EMLP-CNC shown in Fig. 1, which consists of four satellites deployed at the L3, L4, and L5 points and on DRO [9], twenty-eight users evenly distributed across the L3, L4, L5 points and the DRO orbit within Cislunar space, along with three GSs located in Jiamusi, Sanya, and Kashgar. Table V provides the detailed locations of the three GSs. The simulation duration spans 30 days, approximately one regression period of the EMLP-CNC. One reflector period comprises five superframes, with the first superframe corresponding to R-Topo's dynamic phase and the remaining four superframes representing its stable phase. Each satellite in the scenario is equipped with two reflector terminals [15]. Further detailed simulation parameters are summarized in Table IV.

A. Performance of R-Topo

1) *The impact of U_R and L_G* : This section explores the impact of U_R and L_G on the performance of R-Topo. Ground operators set both U_R and L_G , where U_R represents the reflector user requirements and L_G denotes the desired number of RLs to be established with ground stations. By default, we set $\vec{w} = [0.25, 0.25, 0.25, 0.25]$. \vec{w} represents the weight coefficients in the R-Topo optimization objective. Different \vec{w} settings lead to different optimal R-Topo. We investigated the number of NRT users, the average to-GS delay for NRT users, and the average to-GS delay for all reflector users under different values of U_R and L_G by averaging the metrics per reflector period over the entire simulation duration. Here, $|U_R| = X$ indicates that X reflector users have communication needs during a period. Throughout the simulation, U_R remains

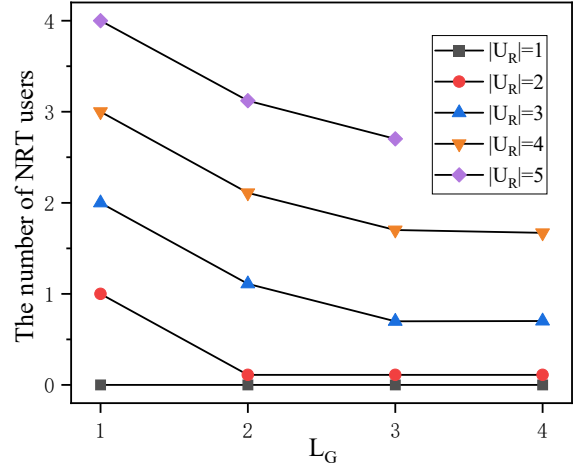


Fig. 7. The number of NRT users vs. L_G

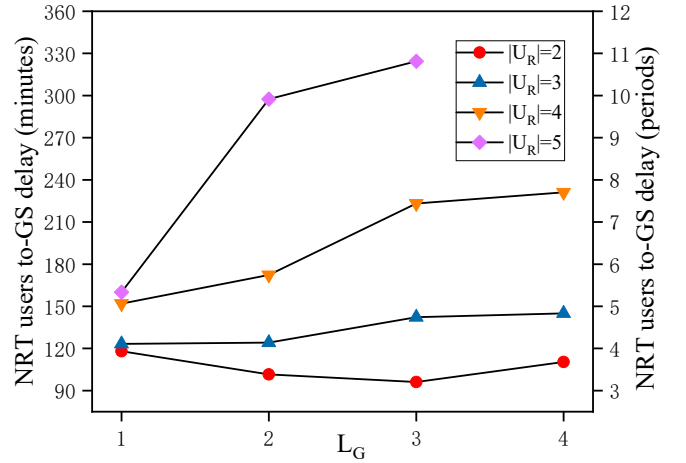


Fig. 8. NRT users to-GS delay vs. L_G

consistent. By default, only one user among the X is required to be an RT user.

Fig. 7 illustrates the curve representing the number of NRT users. When $|U_R| = 1$, the number of NRT users remains zero because the only user in U_R is designated as an RT user. This ensures that R-CPD prioritizes selecting an R-Topo that satisfies U_R . When $|U_R| \geq 2$, as L_G increases, more RL(Sat,GS)s are established, thereby increasing the likelihood of users connecting to G-Sats and becoming RT users. Consequently, the number of NRT users decreases. In scenarios where $|U_R| = 5$ and $L_G = 4$, it is not feasible to satisfy all constraints, resulting in missing data in Fig. 7.

Fig. 8 illustrates the curve of the to-GS delay for NRT users. When $|U_R| = 1$, there are no NRT users; hence, this case is omitted in Fig. 8. When $|U_R| = 2$ or $|U_R| = 3$, the increase in delay is negligible as L_G grows. This is because, with a small $|U_R|$, the number of RL(Sat,User)s remains low, leaving sufficient reflector terminals available to establish RL(UG-Sat,UG-Sat)s. These additional links benefit

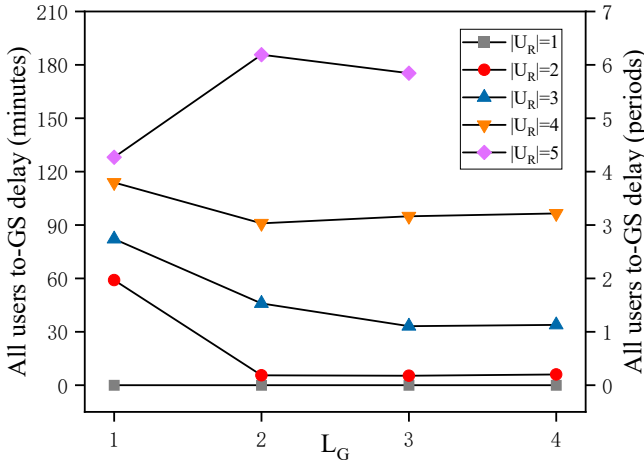


Fig. 9. All users to-GS delay vs. L_G

TABLE VI
IMPACT OF \vec{w} ON THE R-TOPO

\vec{w}	NRT Users to-GS Delay	All Users to-GS Delay
[0.1,0.7,0.1,0.1]	7.058 Periods	3.723 Periods
[0.1,0.1,0.7,0.1]	5.322 Periods	2.807 Periods
[0.1,0.1,0.1,0.7]	5.785 Periods	3.031 Periods
[0.7,0.1,0.1,0.1]	5.885 Periods	3.104 Periods
[0.25,0.25,0.25,0.25]	5.702 Periods	3.007 Periods

NRT users by facilitating data transfer to GSs. For example, if user x is connected to UG-Sat y , and $RL(UG-Sat\ y, UG-Sat\ z)$ exists, x 's data can eventually be relayed to GSs once y or z transitions to a G-Sat in subsequent periods.

However, when $|U_R|$ becomes large, an increase in L_G reduces the availability of terminals to establish $RL(UG-Sat, UG-Sat)$ s. Consequently, the opportunities for UG-Sat y to relay data to GSs via other UG-Sats diminish. In such scenarios, y must become a G-Sat in subsequent periods to complete data transmission. However, due to visibility constraints, y may remain a UG-Sat for extended periods, significantly increasing the to-GS delay for user x connected to y .

Fig. 9 shows the curve for the to-GS delay of all users. When $|U_R|$ is small, an increase in L_G results in more RT users whose delay is zero. This reduces the overall delay for all users. However, when $|U_R|$ is large, the significant deterioration in the to-GS delay of NRT users can outweigh the benefits gained from additional RT users, potentially causing an overall increase in delay for all users.

In conclusion, R-Topo's user service capacity is constrained. For a fixed L_G , a larger $|U_R|$ reduces the available service resources per user, thereby increasing user delay.

2) *The Impact of \vec{w}* : This section examines how \vec{w} influences the performance of R-Topo. Table VI presents the NRT users' to-GS delay and the to-GS delay for all users under $L_G = 2$, $|U_R| = 4$, and various configurations of \vec{w} .

Results in Table VI, $\vec{w} = [0.1, 0.1, 0.7, 0.1]$ demonstrates superior all users to-GS delay performance. Under this parameter, the system targets an optimal R-Topo by constructing

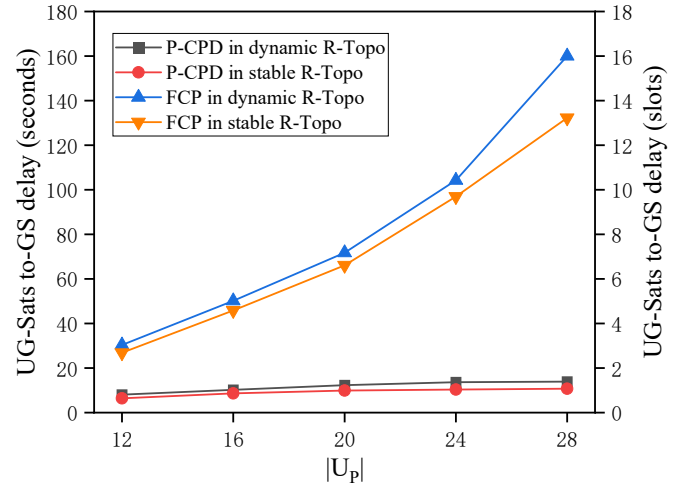


Fig. 10. UG-Sats to-GS delay vs. U_P

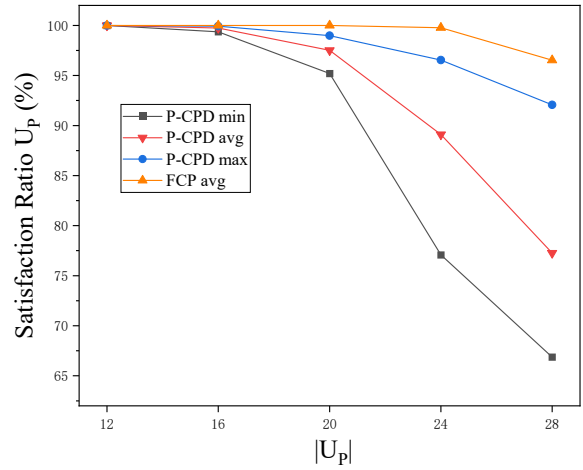


Fig. 11. Satisfaction ratio of U_P vs. U_P

more $RL(Sat, Sat)$ s; the additional $RL(UG-Sat, UG-Sat)$ s lead to lower NRT users to-GS delay, thereby reducing the overall user delay. Among all combinations, $\vec{w} = [0.1, 0.7, 0.1, 0.1]$ performs the worst. This configuration seeks stronger connectivity between satellites and GSs and tends to construct more $RL(IDG-Sat, DG-Sat)$ s while ignoring the construction of $RL(UG-Sat, UG-Sat)$ s when the number of $RL(Sat, GS)$ s is fixed. This results in a higher NRT users to-GS delay, thereby increasing the overall users to-GS delay. $\vec{w} = [0.25, 0.25, 0.25, 0.25]$ represents a balanced choice, achieving suboptimal overall users delay performance.

It is important to note that the data in Table VI is analyzed only under $L_G = 2$, $|U_R| = 4$. Different \vec{w} configurations may exhibit R-Topo performance that differs from TABLE VI for other parameter values. However, $\vec{w} = [0.25, 0.25, 0.25, 0.25]$ can serve as a moderate choice across various scenarios, and all subsequent scenarios will default to this configuration.

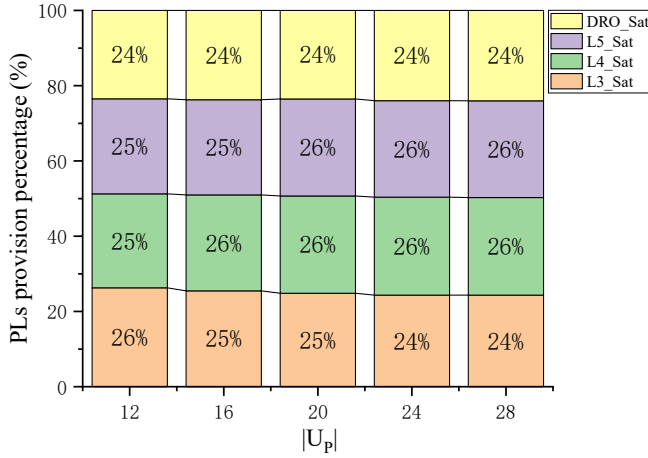


Fig. 12. PLs provision percentage vs. U_P based on P-CPD

B. Performance of P-Topo

We take FCP [22] as a benchmark algorithm to evaluate the performance of P-CPD based on the maximum weight matching algorithm. To adapt FCP to this scenario, we modify it such that once all satellites have provided the required number of PLs for a specific user, FCP will no longer allocate additional PLs. Although FCP is designed to achieve fairness across different applications, the analysis of FCP results demonstrates that the weighted strategy of P-CPD can effectively optimize to-GS delay and meet users' needs as much as possible when applied to EMLP-CNC. This is particularly evident given that FCP also leverages matching algorithms, making the comparison relevant and insightful.

1) *The impact of U_P* : This section explores the impact of U_P on the P-Topo. U_P represents the phased array user requirements set by ground operators. By default, we set $|U_R|=3$, $L_G=2$, and $\vec{C}=[1,2,100]$. \vec{C} is the ranging constant, communication constant, and user service constant in weights assignment for edges. We analyze the to-GS delay of UG-Sats in the P-Topo during the dynamic phase and stable phase of R-Topo, the satisfaction ratio of U_P , and the PL provision percentage of each satellite under different U_P values by averaging these metrics per superframe over the entire simulation duration. Here, $|U_P|=X$ represents X phased array users requiring link establishment within each superframe. We set U_P to remain consistent across all superframes throughout the simulation. By default, each user requires four PLs per superframe from the satellites, i.e., $\forall(x, L_x^u) \in U_P, L_x^u=4$.

Fig. 10 illustrates the to-GS delay for UG-Sats. As $|U_P|$ increases, the delay during both R-Topo's dynamic and stable phases rises. This occurs because the time slot resources available to satellites are finite. A higher $|U_P|$ means satellites must serve more users, reducing the time slot resources allocated for establishing PL(UG-Sat, G-Sat)s. Furthermore, if phased array users access G-Sats, their to-GS delay is zero slots. However, if phased array users access UG-Sats, their to-GS delay approximately equals the to-GS delay of the UG-Sats

they connect to. Thus, the delay shown for UG-Sats in Fig. 10 represents the upper limit of users' to-GS delay in the P-Topo. The connectivity among satellites and between satellites and GSs is poorer during the dynamic phase of R-Topo compared to the stable phase. Consequently, the to-GS delay for UG-Sats in the dynamic phase of R-Topo is consistently higher than that in the stable phase.

Moreover, the to-GS delay of FCP is significantly higher than that of P-CPD. This discrepancy arises because FCP focuses solely on fairness in planning PLs without precisely arranging PL(UG-Sat, G-Sat)s to reduce to-GS delay. From a communication perspective, FCP does not intentionally avoid establishing PL(UG-Sat, UG-Sat)s or PL(G-Sat, G-Sat)s, which reduces the benefits R-Topo provides to P-Topo and leads to inefficient use of time slot resources.

The satisfaction ratio of $|U_P|$ is the average ratio of the number of PL(Sat,User)s provided by satellites to the number of PL(Sat,User)s required by users in U_P across all superframes. Fig. 11 illustrates the minimum, average, and maximum satisfaction ratios for U_P . The minimum and maximum satisfaction ratios pertain to specific users, while the average satisfaction ratio represents all users. In this simulation, if satellites provide four PLs per user in each superframe, the minimum, average, and maximum satisfaction ratios all reach 100%. Using P-CPD, when $|U_P| \leq 20$, the minimum and average satisfaction ratios remain above 95%, indicating that the majority of users' link establishment requirements are met. However, as $|U_P|$ continues to grow, the average and minimum satisfaction ratios decline significantly, highlighting that the satellites' time slot resources are insufficient to serve a large number of phased array users within a single superframe.

The satisfaction ratio of FCP surpasses that of P-CPD. This is because the underlying logic of FCP is based on maximum weight matching, where serving a larger number of users tends to achieve a higher total weight than establishing PLs among satellites. Consequently, FCP prioritizes planning PL(Sat, User)s over P-CPD. The fairness of FCP is evident in its alternating provision of PLs by different satellites to various users. However, due to the significantly higher to-GS delay associated with FCP, it proves unsuitable for this scenario.

The PLs provision percentage is defined as the ratio of the number of PL(Sat, User)s provided by a specific satellite to the total number of PL(Sat, User)s provided by all satellites. Fig. 12 illustrates that, based on P-CPD, the ratio for all four satellites consistently remains around 25% across different $|U_P|$, demonstrating excellent load-balancing capabilities among satellites in providing services to users. In phased array navigation services, distributing PLs from different satellites to users, rather than having the same satellite repeatedly provide PLs, results in improved navigation quality [29]. Due to the orbital characteristics of the DRO satellite orbiting the Moon, its visibility is slightly inferior to that of the other three satellites, causing its provision percentage to fall slightly below 25%.

2) *The Impact of \vec{C}* : We apply maximum weight matching for P-CPD, where \vec{C} directly affects the weights of edges, thus

significantly influencing the allocation of time slot resources among satellites. The time slot resources of the satellites are fixed, and \vec{C} determines the competition for these resources among ranging slots (PL(Sat, Sat)s determined by $w_{i,j,t}^r$), communication slots (PL(UG-Sat, G-Sat)s determined by $w_{i,j,t}^c$), and service slots (PL(Sat, User)s determined by $w_{i,j,t}^u$). This paper assumes $C_3 \gg C_1$ and $C_3 \gg C_2$, meaning that P-CPD prioritizes satisfying ranging slots. After fulfilling the requirements of the ranging slots, different values of C_1 and C_2 result in varying competition for communication and service slots, leading to different performances in metrics such as UG-Sats to-GS delay and the average satisfaction ratio of U_P .

Table VII presents the metrics under $|U_R|=3$, $L_G=2$, $|U_P|=20$, and different \vec{C} . The value of C_3 in \vec{C} is always set to 100. Under a fixed $C_1 = 1$, gradually increasing C_2 significantly reduces the to-GS delay of UG-Sats, while the average satisfaction ratio of U_P decreases by less than five percent. Conversely, under a fixed $C_2 = 1$, gradually increasing C_1 maintains a relatively stable satisfaction ratio, but the to-GS delay of UG-Sats noticeably deteriorates.

From the method of updating $w_{i,j,t}^u$ and $w_{i,j,t}^c$, when C_1 is larger, in the majority of slots within the first half of the superframe, satellites prioritize scheduling service slots. This is because, initially, $w_{i,j,t}^u$ is greater than $w_{i,j,t}^c$ since satellites have not yet provided a significant number of PLs to users. As slots accumulate, $w_{i,j,t}^c$ gradually increases. However, once a communication slot is scheduled, $w_{i,j,t}^c$ sharply drops to $1 \times C_2$, giving $w_{i,j,t}^u$ an advantage again. Consequently, satellites return to prioritizing service slots. In the latter part of the superframe, as satellites have provided all or most PLs to users, $w_{i,j,t}^u$ decreases to a level closer to $w_{i,j,t}^c$. At this stage, satellites schedule more communication slots.

Although the competitiveness of communication slots increases in the latter part of the superframe, it remains weaker than the service slots' dominance in the first half. This results in a higher average to-GS delay for UG-Sats over the entire superframe. However, enhancing C_2 reduces the to-GS delay of UG-Sats without excessively impacting the satisfaction ratio. This improvement arises because $w_{i,j,t}^c$ sharply resets to its initial value after a communication slot is scheduled. At this point, service slots regain their advantage, prompting P-CPD to schedule service slots. As slots accumulate, $w_{i,j,t}^c$ increases linearly with a slope of C_2 , leading P-CPD to schedule communication slots again, repeating this cycle.

Increasing C_2 thus results in a more balanced distribution of communication slots and service slots throughout the superframe.

3) *The impact of U_R* : This section explores the impact of U_R on the performance of P-Topo. By default, we set $L_G = 2$, $|U_P| = 20$, and $\vec{C} = [1, 2, 100]$. We analyze the to-GS delay of UG-Sats in P-Topo during the dynamic and stable phases of R-Topo, as well as the satisfaction ratio of U_P .

Fig. 13 illustrates the UG-Sats to-GS delay. As $|U_R|$ increases, the delay during both the dynamic and stable phases of R-Topo grows. With a constant L_G , a larger $|U_R|$ results in

TABLE VII
THE IMPACT OF \vec{C} ON THE P-TOPO

\vec{C}	UG-Sats to-GS-delay	Average satisfaction ratio of U_P
[1,1,100]	2.24863 slots	99.86449 %
[1,2,100]	1.04098 slots	97.50622 %
[1,3,100]	0.74351 slots	96.32095 %
[2,1,100]	4.04138 slots	99.88114 %
[3,1,100]	5.41296 slots	99.8344 %

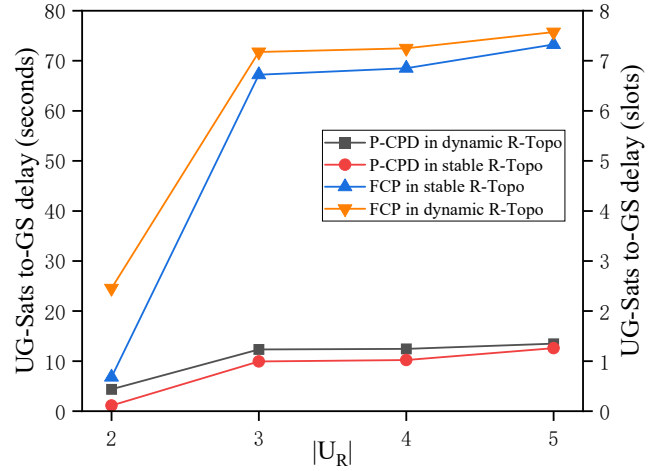


Fig. 13. UG-Sats to-GS delay vs. U_R

satellites building more RL(Sat,User)s, leaving fewer terminals available for RL(Sat,Sat)s. This reduction in RL(Sat,Sat)s diminishes the benefits that R-Topo provides to P-CPD, leading to increased delays.

Although FCP does not fully utilize the connectivity advantages provided by R-Topo, the additional connectivity still aids in reducing the to-GS delay for UG-Sats. Consequently, as $|U_R|$ increases, the delay of FCP also rises significantly.

Fig. 14 demonstrates the minimum, average, and maximum

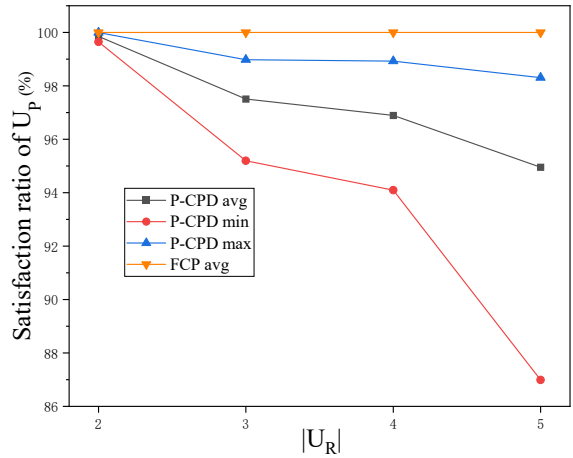


Fig. 14. Satisfaction ratio of U_P vs. U_R

satisfaction ratios of U_P . Based on P-CPD, as $|U_R|$ increases, the number of RL(Sat,Sat)s decreases. During P-CPD, more slot resources must be allocated to satisfy the communication needs of UG-Sats, which reduces the resources available for serving users. This highlights a competitive relationship between reflector users and phased array users under fixed satellite terminal resources. The more reflector users are served by satellites, the weaker the connectivity among satellites (as reflected in R-Topo), forcing satellites to schedule more communication slots (in P-Topo) and thereby diminishing their service capability for phased array users.

In contrast, FCP, aiming to achieve maximum weight, consistently prioritizes serving users, maintaining a high satisfaction ratio. However, it fails to effectively balance communication needs and user service, leading to inefficiencies in connectivity management.

Furthermore, L_G and \vec{w} influence the R-Topo, which subsequently affects P-CPD. Due to space constraints, these aspects are not elaborated on here.

C. Further Discussion

In summary, the impact of all parameters on R-Topo and P-Topo performance confirms the following:

- 1) The R-Topo's ability to serve reflector users is inherently limited, highlighting competition between RT and NRT users. Increasing the number of RL(Sat,GS)s raises the number of RT users but also leads to higher to-GS delays for NRT users in R-Topo.
- 2) The finite time slot resources of satellites create a trade-off between communication and service slots. Proper adjustment of \vec{C} can optimize both the satisfaction ratio of all users and the to-GS delay for UG-Sats in P-Topo.
- 3) Reflector users and phased array users compete for the overall terminal resources of satellites. Reflector users occupy reflector terminals, whereas phased array users benefit when reflector terminals are utilized to construct RL(Sat,GS)s and RL(Sat,Sat)s. Improved connectivity in R-Topo reduces UG-Sats' dependency on communication slots, thereby freeing up more time slot resources for phased array users.
- 4) P-CPD aims to balance user service with the ranging and communication needs of satellites, making it more suitable for EMLP-CNC than FCP, which prioritizes serving users but overlooks the fundamental needs of satellites.
- 5) The essence of CPD lies in the allocation of satellite terminal resources. With limited terminals, the user service capacity of satellites remains constrained. Increasing the number of satellites or equipping each satellite with additional terminals can enhance the service capacity.

VII. CONCLUSIONS

Satellites can be deployed at the libration points of the Earth-Moon system to construct a Cislunar Space Infrastructure. In this paper, we study the CPD problem in EMLP-CNC, aiming to satisfy satellites' ranging and communication needs

while also serving spatial users. Since satellites are equipped with reflector and phased array terminals, we discuss the CPD for the R-Topo and P-Topo separately. We employ LAA-PM to generate an optimal R-Topo that satisfies the communication needs of reflector users. Based on the optimal R-Topo, we implement a P-CPD using maximum weight matching to meet satellites' ranging and communication needs while providing communication and navigation services to phased array users. Performance analyses of R-Topo and P-Topo demonstrate the finite nature of satellites' terminal resources. Under these constraints, competition arises among users and between the diverse objectives of satellites. Our simulations confirm the effectiveness of the R-CPD and P-CPD algorithms presented in this paper, providing strong technical support for constructing a Cislunar Space Infrastructure.

However, this paper's proposed R-CPD and P-CPD algorithms focus exclusively on addressing communication needs for transmitting data to GSs. A comprehensive Cislunar Space Infrastructure should facilitate data transmission from any source to any destination. Although the CPD algorithms discussed in this paper exhibit adaptability for user-to-user communication, they are not fully optimized for such scenarios. In the future, we will aim to design CPD algorithms that address communication requirements from any source to any destination, advancing the Cislunar Space Infrastructure into a fully integrated engineering facility offering foundational and general services [38].

ACKNOWLEDGMENT

This research received support from...

REFERENCES

- [1] S. Creech, J. Guidi, and D. Elburn, "Artemis: an overview of nasa's activities to return humans to the moon," in *2022 IEEE Aerospace Conference (Aero)*. IEEE, 2022, pp. 1–7.
- [2] NASA. (2020) NASA's Lunar Exploration Program Overview. https://www.nasa.gov/sites/default/files/atoms/files/artemis_plan-20200921.pdf.
- [3] X. Ma, X. Dong, and Y. Hu, "Analysis on navigation accuracy of high orbit spacecraft based on bds geo and igso satellites," *Advances in Space Research*, vol. 71, no. 5, pp. 2481–2492, 2023.
- [4] L. B. Winternitz, W. A. Bamford, A. C. Long, and M. Hassouneh, "Gps based autonomous navigation study for the lunar gateway," in *Annual American Astronautical Society (AAS) Guidance, Navigation, and Control Conference*, no. AAS 19-096, 2019.
- [5] F. Pereira and D. Selva, "Exploring the design space of lunar gnss in frozen orbit conditions," in *2020 IEEE/ION Position, Location and Navigation Symposium (PLANS)*. IEEE, 2020, pp. 444–451.
- [6] D. J. Israel, K. D. Mauldin, C. J. Roberts, J. W. Mitchell, A. A. Pulkkinen, D. C. La Vida, M. A. Johnson, S. D. Christe, and C. J. Gramling, "Lunaret: a flexible and extensible lunar exploration communications and navigation infrastructure," in *2020 IEEE Aerospace Conference*. IEEE, 2020, pp. 1–14.
- [7] J. A. Vedda, "Cislunar development: What to build and why," *The Aerospace Corporation*, 2018.
- [8] C. Short, K. Howell, and X. Tricoche, "Lagrangian coherent structures in the restricted three-body problem," in *Proceedings of 21st AAS/AIAA Space Flight Mechanics Meeting, New Orleans, Louisiana, Paper No. AAS, 2011*, pp. 11–250.
- [9] Z. Xu, K. Shao, D. Gu, L. Tong, L. Du, C. Wei, Z. An, and J. Zhu, "Orbit determination of earth-moon libration point navigation constellation based on inter-satellite links," *Advances in Space Research*, vol. 74, no. 2, pp. 937–948, 2024.

- [10] Y. Gao, C. Hu, Y. Xin, K. Jiang, B. Xu, B. Wang, and J. Zhou, "Design of a cislunar space navigation constellation based on special long-period orbits," *Advances in Space Research*, 2024.
- [11] J. R. Carpenter, D. Folta, M. Moreau, and D. Quinn, "Libration point navigation concepts supporting the vision for space exploration," in *AIAA/AAS Astrodynamics Specialist Conference and Exhibit*, 2004, p. 4747.
- [12] L. Liu, W.-R. Wu, and Y. Liu, "Design and implementation of chinese libration point missions," *Science China Information Sciences*, vol. 66, no. 9, p. 191201, 2023.
- [13] Z.-Y. Gao and X.-Y. Hou, "Coverage analysis of lunar communication/navigation constellations based on halo orbits and distant retrograde orbits," *The Journal of Navigation*, vol. 73, no. 4, pp. 932–952, 2020.
- [14] Y. Gao, Z. You, J. Liu, and B. Xu, "The influence of orbital maneuver on autonomous orbit determination of an extended satellite navigation constellation," *Advances in Space Research*, vol. 67, no. 6, pp. 1733–1742, 2021.
- [15] Y. Rahmat-Samii and R. Haupt, "Reflector antenna developments: a perspective on the past, present and future," *IEEE Antennas and Propagation Magazine*, vol. 57, no. 2, pp. 85–95, 2015.
- [16] C. Wang, Y. Wang, P. Lian, S. Xue, Q. Xu, Y. Shi, Y. Jia, B. Du, J. Liu, and B. Tang, "Space phased array antenna developments: A perspective on structural design," *IEEE Aerospace and Electronic Systems Magazine*, vol. 35, no. 7, pp. 44–63, 2020.
- [17] A. Meguro, K. Shintate, M. Usui, and A. Tsujihata, "In-orbit deployment characteristics of large deployable antenna reflector onboard engineering test satellite viii," *Acta Astronautica*, vol. 65, no. 9-10, pp. 1306–1316, 2009.
- [18] D. Semler, A. Tulintseff, R. Sorrell, and J. Marshburn, "Design, integration, and deployment of the terestar 18-meter reflector," in *28th AIAA International Communications Satellite Systems Conference (ICSSC-2010)*, 2010, p. 8855.
- [19] J. A. Fraire and J. M. Finochietto, "Design challenges in contact plans for disruption-tolerant satellite networks," *IEEE Communications Magazine*, vol. 53, no. 5, pp. 163–169, 2015.
- [20] J. Fraire and J. M. Finochietto, "Routing-aware fair contact plan design for predictable delay tolerant networks," *Ad Hoc Networks*, vol. 25, pp. 303–313, 2015.
- [21] J. A. Fraire, P. G. Madoery, and J. M. Finochietto, "Traffic-aware contact plan design for disruption-tolerant space sensor networks," *Ad Hoc Networks*, vol. 47, pp. 41–52, 2016.
- [22] J. A. Fraire and P. G. Madoery, "On the design and analysis of fair contact plans in predictable delay-tolerant networks," *IEEE Sensors Journal*, vol. 14, no. 11, pp. 3874–3882, 2014.
- [23] Z. Yan, G. Gu, K. Zhao, Q. Wang, G. Li, X. Nie, H. Yang, and S. Du, "Integer linear programming based topology design for gnss with inter-satellite links," *IEEE Wireless Communications Letters*, vol. 10, no. 2, pp. 286–290, 2020.
- [24] Z. Yan, J. A. Fraire, K. Zhao, H. Yan, P. G. Madoery, W. Li, and H. Yang, "Distributed contact plan design for gnss," *IEEE Transactions on Aerospace and Electronic Systems*, vol. 56, no. 1, pp. 660–672, 2019.
- [25] Z. Yan, K. Zhao, W. Li, C. Kang, J. Zheng, H. Yang, and S. Du, "Topology design for gnss under polling mechanism considering both inter-satellite links and ground-satellite links," *IEEE Transactions on Vehicular Technology*, vol. 71, no. 2, pp. 2084–2097, 2021.
- [26] Z. Hou, X. Yi, Y. Zhao, C. Li, and Y. Xie, "Contact plan design for navigation satellite network based on maximum matching," in *Proceedings of the 2nd International Conference on Vision, Image and Signal Processing*, 2018, pp. 1–6.
- [27] L. Sun, Y. Wang, W. Huang, J. Yang, Y. Zhou, and D. Yang, "Inter-satellite communication and ranging link assignment for navigation satellite systems," *Gps Solutions*, vol. 22, pp. 1–14, 2018.
- [28] J. Yan, L. Xing, P. Wang, L. Sun, and Y. Chen, "A scheduling strategy to inter-satellite links assignment in gnss," *Advances in Space Research*, vol. 67, no. 1, pp. 198–208, 2021.
- [29] H. Yan, Q. Zhang, Y. Sun, and J. Guo, "Contact plan design for navigation satellite network based on simulated annealing," in *2015 IEEE International Conference on Communication Software and Networks (ICCSN)*. IEEE, 2015, pp. 12–16.
- [30] D. Yang, J. Yang, and P. Xu, "Timeslot scheduling of inter-satellite links based on a system of a narrow beam with time division," *Gps Solutions*, vol. 21, pp. 999–1011, 2017.
- [31] H. Kai, X. Bingbing, S. Fengwei, G. Wenbin, and R. Qianyi, "An adaptive topology optimization strategy for gnss inter-satellite network," *Authorea Preprints*, 2023.
- [32] J. Huang, Y. Su, W. Liu, and F. Wang, "Optimization design of inter-satellite link (isl) assignment parameters in gnss based on genetic algorithm," *Advances in space research*, vol. 60, no. 12, pp. 2574–2580, 2017.
- [33] J. Yan, G. Song, R. Leus, Z. Hou, and Z. Zhang, "Rolling weight-matching methods for the inter-satellite link assignment in global navigation satellite systems," *Gps Solutions*, vol. 26, no. 2, p. 38, 2022.
- [34] Z. Liu, W. Guo, C. Deng, W. Hu, H. Chen, Y. Zhao, and M. Xia, "Perfect match model based link assignment for optical satellite network," in *2014 IEEE International Conference on Communications (ICC)*. IEEE, 2014, pp. 4149–4153.
- [35] L. Lovász and M. D. Plummer, *Matching theory*. American Mathematical Soc., 2009, vol. 367.
- [36] P. Giordano, F. Malman, R. Swinden, P. Zoccarato, and J. Ventura-Traveset, "The lunar pathfinder pnt experiment and moonlight navigation service: The future of lunar position, navigation and timing," in *Proceedings of the 2022 International Technical Meeting of The Institute of Navigation*, 2022, pp. 632–642.
- [37] M. Murata, I. Kawano, and S. Kogure, "Lunar navigation satellite system and positioning accuracy evaluation," in *Proceedings of the 2022 International Technical Meeting of The Institute of Navigation*, 2022, pp. 582–586.
- [38] M. F. Yang, J. Peng, J. H. Li *et al.*, "Architecture and development envision of cislunar space infrastructure," *Chinese Space Science and Technology*, vol. 44, no. 3, pp. 1–14, 2024.
- [39] J.-C. Angevain, A. Ihle, G. Rodrigues, and J. Santiago-Prowald, "Large deployable spaceborne reflector antennas in europe: progress status and perspectives," in *2019 13th European Conference on Antennas and Propagation (EuCAP)*. IEEE, 2019, pp. 1–5.
- [40] S. Qin, Y. Huang, P. Li, Q. Shan, M. Fan, X. Hu, and G. Wang, "Orbit and tracking data evaluation of chang'e-4 relay satellite," *Advances in Space Research*, vol. 64, no. 4, pp. 836–846, 2019.
- [41] M. Fan, X. Hu, G. Dong, Y. Huang, J. Cao, C. Tang, P. Li, S. Chang, and Y. Yu, "Orbit improvement for chang'e-5t lunar returning probe with gnss technique," *Advances in Space Research*, vol. 56, no. 11, pp. 2473–2482, 2015.
- [42] Y.-H. Meng and Q.-F. Chen, "Outline design and performance analysis of navigation constellation near earth-moon libration point," 2014.
- [43] S. R. Pratt, R. A. Raines, C. E. Fossa, and M. A. Temple, "An operational and performance overview of the iridium low earth orbit satellite system," *IEEE Communications Surveys*, vol. 2, no. 2, pp. 2–10, 1999.
- [44] D. Bhattacharjee and A. Singla, "Network topology design at 27,000 km/hour," in *Proceedings of the 15th International Conference on Emerging Networking Experiments And Technologies*, 2019, pp. 341–354.
- [45] X. Qi, B. Zhang, Z. Qiu, and L. Zheng, "Using inter-mesh links to reduce end-to-end delay in walker delta constellations," *IEEE Communications Letters*, vol. 25, no. 9, pp. 3070–3074, 2021.
- [46] J. Pi, Y. Ran, H. Wang, Y. Zhao, R. Zhao, and J. Luo, "Dynamic planning of inter-plane inter-satellite links in leo satellite networks," in *ICC 2022-IEEE International Conference on Communications*. IEEE, 2022, pp. 3070–3075.
- [47] H. S. Chang, B. W. Kim, C. G. Lee, S. L. Min, Y. Choi, H. S. Yang, D. N. Kim, and C. S. Kim, "Fsa-based link assignment and routing in low-earth orbit satellite networks," *IEEE transactions on vehicular technology*, vol. 47, no. 3, pp. 1037–1048, 1998.
- [48] S. Liu, J. Yang, X. Guo, and L. Sun, "Inter-satellite link assignment for the laser/radio hybrid network in navigation satellite systems," *GPS Solutions*, vol. 24, pp. 1–14, 2020.
- [49] D. Yang, J. Yang, G. Li, Y. Zhou, and C. Tang, "Globalization highlight: orbit determination using beidou inter-satellite ranging measurements," *GPS Solutions*, vol. 21, pp. 1395–1404, 2017.
- [50] J. A. Fraire, O. De Jonckère, and S. C. Burleigh, "Routing in the space internet: A contact graph routing tutorial," *Journal of Network and Computer Applications*, vol. 174, p. 102884, 2021.
- [51] V. Cerf *et al.*, "Delay-Tolerant Networking Architecture," <http://www.rfc-editor.org/rfc/rfc4838.txt>, RFC Editor, April 2007, RFC 4838.
- [52] G. Schäfer, "Weighted matchings in general graphs," Master's thesis, Universität des Saarlandes, Saarbrücken, Germany, 2000.